

Accepted Manuscript

Layer-specific Diffusion Weighted Imaging in human primary visual cortex *in vitro*

Michiel Kleinnijenhuis, Valerio Zerbi, Benno Küsters, Cornelis H. Slump, Markus Barth, Anne-Marie van Cappellen van Walsum



PII: S0010-9452(12)00334-6

DOI: [10.1016/j.cortex.2012.11.015](https://doi.org/10.1016/j.cortex.2012.11.015)

Reference: CORTEX 946

To appear in: *CORTEX*

Received Date: 29 March 2012

Revised Date: 16 October 2012

Accepted Date: 24 November 2012

Please cite this article as: Kleinnijenhuis M, Zerbi V, Küsters B, Slump CH, Barth M, Walsum A-MvCv, Layer-specific Diffusion Weighted Imaging in human primary visual cortex *in vitro*, *CORTEX* (2013), doi: 10.1016/j.cortex.2012.11.015.

This is a PDF file of an unedited manuscript that has been accepted for publication. As a service to our customers we are providing this early version of the manuscript. The manuscript will undergo copyediting, typesetting, and review of the resulting proof before it is published in its final form. Please note that during the production process errors may be discovered which could affect the content, and all legal disclaimers that apply to the journal pertain.

Title:

Layer-specific Diffusion Weighted Imaging in human primary visual cortex *in vitro*

Authors:

Michiel Kleinnijenhuis^{1,2}, Valerio Zerbi^{1,3}, Benno Küsters⁴, Cornelis H. Slump⁶, Markus Barth^{2,5} and Anne-Marie van Cappellen van Walsum^{1,6}

Affiliation:

¹Department of Anatomy, Radboud University Nijmegen Medical Centre, Nijmegen, Netherlands

²Radboud University Nijmegen, Donders Institute for Brain, Cognition and Behaviour, Nijmegen, Netherlands

³Department of Radiology, Radboud University Nijmegen Medical Centre, Nijmegen, Netherlands

⁴Department of Pathology, Radboud University Nijmegen Medical Centre, Nijmegen, Netherlands

⁵Erwin L. Hahn Institute for Magnetic Resonance Imaging, Essen, Germany

⁶MIRA Institute for Biomedical Technology and Technical Medicine, University of Twente, Netherlands

Abbreviated title:

Layer-specific DWI in human V1 *in vitro*

Corresponding author:

Anne-Marie van Cappellen van Walsum
Radboud University Nijmegen Medical Centre
Department of Anatomy
Huispost 109 Anatomie
Postbus 9101
6500 HB Nijmegen
The Netherlands
T: 0031 (0)24 36 13341
F: 0031 (0)24 36 13789
E: A.vanCappellenvanWalsum@anat.umcn.nl

Abstract:

One of the most prominent characteristics of the human neocortex is its laminated structure. The first person to observe this was Francesco Gennari in the second half the 18th century: in the middle of the depth of primary visual cortex, myelinated fibres are so abundant that he could observe them with bare eyes as a white line. Because of its saliency, the stria of Gennari has a rich history in cyto- and myeloarchitectural research as well as in magnetic resonance (MR) microscopy. In the present paper we show for the first time the layered structure of the human neocortex with *ex vivo* diffusion weighted imaging (DWI). To achieve the necessary spatial and angular resolution, primary visual cortex samples were scanned on an 11.7 T small-animal MR system to characterize the diffusion properties of the cortical laminae and the stria of Gennari in particular. The results demonstrated that fractional anisotropy varied over cortical depth, showing reduced anisotropy in the stria of Gennari, the inner band of Baillarger and the deepest layer of the cortex. Orientation density functions showed multiple components in the stria of Gennari and deeper layers of the cortex. Potential applications of layer-specific diffusion imaging include characterization of clinical abnormalities, cortical mapping and (intra)cortical tractography. We conclude that future high-resolution *in vivo* cortical DWI investigations should take into account the layer-specificity of the diffusion properties.

Keywords:

Diffusion Weighted Imaging, cortical anisotropy, layer-specific, primary visual cortex, stria of Gennari

Acknowledgement

The research was funded by Ministerie van Economische Zaken, Provincie Overijssel and Provincie Gelderland through the ViP-BrainNetworks project; and the Bruker BioSpec 11.7T NWO middelgroot nr. 40-00506-90-0602 and NWO BIG (VISTA) investment grants to A. Heerschap. The authors express their gratitude to Andor Veltien, David Norris and Dirk Ruiten for their advisory support in this project.

Abbreviations

V1 = primary visual cortex, BA = Brodmann area, MRI = magnetic resonance imaging, DWI = diffusion weighted imaging, MR = magnetic resonance, MGE = multi-echo gradient echo, FA = fractional anisotropy, FOD = fibre orientation distribution, GM = grey matter, L1-L3 = tensor eigenvalues, WM = white matter

1 Introduction

The human cortex is not a homogeneous structure. Francesco Gennari must have been tremendously excited when he first discovered this in 1776 as a 23-year old medical student. Under the impression that he found a third brain substance in the iced brains he was investigating, Gennari described a set of white lines running parallel to the cortical surface—two lines in some locations, only one elsewhere. Although he observed the phenomenon throughout the cortex, it was most prominent in the medial portion of the occipital lobe (Gennari, 1872; Figure 1b). Nowadays, we know this region to be the primary visual cortex (V1). It is consistently located in the depth of the calcarine sulcus and is further characterized by an abundance of transverse myelinated fibres in cortical layer IVb: the stria of Gennari. His name was not given to the feature until a century after his discovery, because the more eminent contemporary scientist Félix Vicq d'Azyr laid claim to it. Sadly, Gennari's talents as an anatomist seem to have dwindled after publication of his first and only book as the result of his gambling habits (Glickstein and Rizzolatti, 1984).

With the limited knowledge of brain function in his day and age, Gennari could not have fathomed what his discovery signified. It is the anatomical basis of the two most important principles of functional specialization in the brain: 1) that the cortex is a laminated structure in which every layer serves specific functions in neuronal processing; and 2) that the cortical sheet comprises functionally specialized areas that differentiate in their laminar anatomy.

[Insert Figure 1 here]

In the first half of the 19th century, the gross anatomy underlying the first principle was further investigated by Jules Baillarger (Figure 2a) who established that the mammalian neocortex is composed of six layers of alternating grey and white appearance (Baillarger, 1840). Although his six layers differ from the six layers as they are presently defined, the 'inner and outer bands of Baillarger' are still features of the cortex often referred to today (Figure 2b). Baillarger rightly dismissed the existence of Gennari's third brain substance, but failed to appreciate that his 'outer band' was actually the exact same line that Gennari saw. He ascribed the whitish opaque layers of his illuminated transparent cortical sections to thickened radial fibres continuous with the white matter. Although he mentioned transverse fibres forming a grid with these radial fibres, he did not realise that these actually formed the conspicuous white bands.

Genuine breakthroughs in the correct characterization of these layers could be expected only after the development of adequate histological methods. The discovery of formalin fixation methods (Blum, 1893) and dyes with specific affinity for neurons (Golgi, 1873) and myelin (Weigert, 1884) opened up a whole new playing field that we know as cortical architectonics. Through the pioneering work of Theodor Meynert (Figure 2c)—the first scientist to employ these techniques efficiently—the realization emerged that a distinct layered cytological fingerprint can be found over the depth of the cortex that varies over cortical areas—a century after Gennari saw the first clues. While Meynert recognized that most of the cortical areas have six layers, he identified eight layers in the primary visual cortex (Figure 2d). Many classifications of the cytological fingerprint were proposed in the following decades, as well as many cyto- and myeloarchitectonic maps. Of these, Korbinian

Brodmann's classification scheme (Brodmann, 1905) and map (Brodmann, 1909) have proven to be the most lasting, as they are still widely used today.

[Insert Figure2 here]

The primary visual cortex was listed by Brodmann as area 17 (BA17). It has had a rather special role in cortical architectonics, because of the distinct feature of the stria of Gennari: the only laminar cortical phenomenon visible with the bare eye. The transition of the cytoarchitectural fingerprint to that of the cortical area that surrounds it (BA18) is rather abrupt. Therefore, of all cortical areas, V1 is easiest to delineate anatomically. Together with its well-defined receptive field properties, this has made V1 the most investigated area of the cortex. With the advent of magnetic resonance imaging (MRI), a tool is available for measuring the cortical cyto- and myeloarchitecture *in vivo*: one of the main aims of neuroscience today. Various contrasts have been employed for this purpose, most providing insights on myelination of cortical areas. Therefore, the heavily myelinated stria of Gennari makes V1 also the most popular target for laminar MRI investigations (Barbier et al., 2002; Blackwell et al., 2009; Bridge et al., 2005; Koopmans et al., 2008, 2010; Trampel et al., 2011; Turner et al., 2008).

Although diffusion weighted imaging (DWI) also appears to be a promising tool for imaging the cortical architecture, it has been largely ignored in cortical investigations due to anatomical characteristics and technical limitations. Conversely, DWI has been mainly used to investigate white matter, because it has a relatively coherent organization at the scale of the DWI voxel. The accumulation of axons in fibre bundles results in marked diffusion anisotropy, where the Brownian motion of water molecules is less hindered by biological boundaries along the axonal direction in comparison to perpendicular to the axons. Nevertheless, adequate reconstruction of the underlying architecture on the basis of these measurements is far from straightforward, even in white matter, because of the ambiguous diffusion profile resulting from multiple fibre bundles included in most DWI voxels. For the grey matter, resolving neuronal architecture from a diffusion experiment is even more complex as there are additional neuronal constituents (including somata, dendrites and axons) and cell types to take into account. These have an enormous diversity in shapes and sizes, not at all as neatly bundled as the axons in white matter.

In the cortex, an additional challenge is that the typical spatial resolution of *in vivo* DWI is an order of magnitude larger than any single cortical layer, i.e. the depth of the cortex is typically spanned by only 1-2 voxels of ~2 mm. The diffusion profile seen in any cortical voxel will therefore be a superposition of the profiles of several, if not all, cortical layers in addition to any partial volume with white matter or cerebrospinal fluid in the subarachnoid space. Recently, high-resolution DWI investigations have been performed showing anisotropic diffusion in human neocortex in a predominantly radial orientation to the cortical surface (Heidemann et al., 2010; Jaermann et al., 2008; McNab et al., 2009). For tractography—i.e. reconstructing the most likely fibre pathways underlying the diffusion measurement—this implies a major improvement. In a typical DWI dataset fibres cannot be traced to their cortical terminations, because the cortical voxels lack robust anisotropy in the diffusion profile. The radial cortical anisotropy observed at high resolution expands the range of the tractography technique to the cortex, such that streamlines can be tracked more specifically to a cortical patch by following the radial direction over the white-grey matter boundary.

With the advance to higher resolutions and the possibility to include the cortex in human *in vivo* DWI investigations, there is need for better characterization of the MR diffusion properties of cortical voxels. Our hypothesis is that every cortical layer has distinct diffusion properties that reflect radially and tangentially oriented neural processes. This has not been investigated previously in sufficient detail. To acquire DWI at the spatial and angular resolution required to differentiate and characterize cortical layers, we investigated *ex vivo* human cortical tissue samples on an 11.7T small-animal MR system. Primary visual cortex samples were selected, because the contribution of tangential fibres is expected to be most pronounced in the stria of Gennari.

2 Methods

2.1 Sample preparation

Two human brain tissue samples were obtained at autopsy. The post-mortem interval between death and sample acquisition was kept as short as possible (21 hours) to avoid tissue degradation from autolytic processes (D'Arceuil and de Crespigny, 2007). Blocks of tissue ($\sim 20 \times 20 \times 20$ mm) were excised from the brain to ensure fast penetration of the fixative solution. The blocks were cut around the calcarine sulcus and included the underlying white matter. Sample A was the occipital pole. Sample B consisted of both the upper and lower bank of the sulcus. The tissue was stored (> 6 months) at 4°C in 50 ml vials filled with 4 % buffered formaldehyde solution. Before magnetic resonance imaging, the samples were rehydrated in phosphate buffered saline (> 2 weeks) to reduce fixation-induced T2 shortening (Shepherd et al., 2009). Twenty-four hours prior to MRI, the samples were transferred to a syringe filled with Galden D40 perfluoropolyether (Solvay Solexis, New York) at room temperature. This facilitated the expulsion of air bubbles from the sample.

2.2 MRI data acquisition

MR measurements were performed on the samples in the syringe on a 11.7 T BioSpec Avance III small animal MR system (Bruker BioSpin, Ettlingen, Germany) equipped with an actively shielded gradient set of 600 mT/m (slew rate 4570 T/m/sec). A circular polarized resonator was used for signal transmission and an actively-decoupled mouse brain coil for receiving (Bruker BioSpin). Diffusion weighted images were acquired with a spin-echo protocol ($\text{TR}=13.75$ s; $\text{TE}=26.6$ ms) using segmented echo-planar readout (4 segments). Diffusion gradients were applied with a b-value of 4000 sec/mm^2 ($\delta = 4$ msec; $\Delta = 12.5$ msec). The field-of-view covered the sample (28.8×28.8 mm) and was sampled with a 96×96 matrix leading to a 0.3×0.3 mm in-plane resolution. The slice thickness was 0.3 mm resulting in isotropic voxels. Sample A was measured with 55 slices, 61 diffusion directions equally distributed over the hemisphere (Cook et al., 2007), 7 non-diffusion weighted images and 14 repetitions. Sample B was measured with 70 slices, 768 diffusion directions equally distributed over the sphere (Jones et al., 1999), 64 non-diffusion weighted images and 1 repetition. Signal-to-noise ratio for the $b=0$ images ranged from 90 in the grey matter directly under the coil to 40 in the white matter 3 mm below the grey-white matter boundary. Multi-echo gradient-echo images (MGE) were acquired in both samples for anatomical reference of cortical architecture. They were obtained with a 3D FLASH sequence reading 5 echoes at evenly spaced intervals between $\text{TE} = 3.36$ - 38.36 msec. Imaging parameters were: $\text{TR} = 40$ msec; $\alpha = 30^\circ$, field-of-view $28.8 \times 28.8 \times 28.8$ mm sampled with a $256 \times 256 \times 256$ matrix, resulting in 0.11 mm isotropic voxels. Total acquisition time for each sample was approximately 14 hours.

2.3 MRI data analysis

The five MGE echoes were averaged and divided by the coil sensitivity profile. The same procedure was followed for the non-diffusion weighted volumes. The diffusion weighted volumes were corrected for eddy currents by affine coregistration to the first non-diffusion weighted volume (FSL FLIRT). Using the PATCH toolbox (Zwiers, 2010), the corrected mean of the non-diffusion weighted

volumes was coregistered and unwarped (Visser et al., 2010) to the corrected mean of the MGE echoes. The affine and unwarping transformations were applied to all diffusion weighted volumes.

The preprocessed DWI volumes were analyzed with MRtrix (v.0.2.9), reconstructing maps of fractional anisotropy (FA), mean diffusivity (MD), diffusion tensor eigenvalues (L1-L3) and directionally encoded colourmaps (DEC). Fiber orientation distributions (FODs) were reconstructed by performing constrained spherical deconvolution (CSD; Tournier et al., 2007) with a maximum harmonic order of 8. The fiber response function was estimated from the (~7000) voxels with $FA > 0.1$ within a mask with high SNR and excluding pial boundary voxels. To obtain profiles of diffusion metrics over the cortical depth, MRtrix deterministic CSD tractography was performed seeding from MGE voxels on the pial surface. For each sample, we selected a flat patch (with diameter of 1.7 mm (=15 MGE voxels) in which cortical thickness was assumed equal) of V1 cortex that showed the stria of Gennari in the MGE image and a patch of V2 cortex that did not. A fixed initial tracking direction perpendicular to the cortex was specified and streamlines were traced (with a stepsize of 0.03 mm and FOD amplitude constraint of 0.02) until 10000 fibres were found with a length larger than 1 mm. The MGE, FA, MD, L1-L3 maps were sampled at each point along the streamlines. Additional results of an alternative approach sampling the profiles along the cortex normals can be found in Supplementary Figure 1.

3 Results

In all maps of MGE and diffusion tensor metrics a distinct layered structure can be observed in primary visual cortex (Figures 3 and 4 for samples A and B). In the MGE image (Figure 3,4ag), the white matter has a dark patchy appearance and u-fibres can be observed as dark curves closely following the GMWM boundary. The cortex has a layered appearance, with the stria of Gennari as a band of low intensity approximately halfway the cortical depth. The stria of Gennari is not visible throughout the cortex, indicating that the samples also contain V2 cortex. The dashed lines in the MGE images show the V1/V2 transitions. Close inspection reveals a second dark cortical layer in the MGE (indicated by the arrows in Figure 4g).

[Insert Figures 3 and 4 here]

The MD map appears very similar to the MGE. In V1, a dark band (two bands in some locations) of low diffusivity runs parallel to the cortical surface. In the white matter, the MD also resembles the MGE, with u-fibres exhibiting low diffusivity (e.g. arrow Figure 3b). Also the FA maps clearly reveal the layered structure of the primary visual cortex (arrows highlight some bands of low FA). Including the band of low FA on the GMWM boundary, some areas show three bands, while in other areas only two are apparent. With the exception of the low intensity band at the GMWM boundary, we do not observe this pronounced stack of layers in V2. The DEC maps illustrate the wide range of fiber directions in these small samples.

Fiber orientation distribution functions are presented for cortical areas V1 (Figure3,4ekl) and V2 (Figure3,4f). The main orientation in the cortex is radial to the cortical surface. The direction in the WM directly underlying the cortex is generally tangential to the cortical sheet, with the exception of gyral crowns. In Figure4e intermediate main orientations can be seen at the GMWM boundary where the fibres do not bend sharply, but appear to gradually fan out into the cortex. On the GMWM boundary, multicomponent FODs are reconstructed. This layer extends over multiple voxels into the deep cortical layers, suggesting that partial volume between WM u-fibres and radial cortical fibres is not the only underlying mechanism. Going outward towards the pial surface, the typical pattern in V1 then shows a band with increased radially, followed by a band with complex multicomponent FODs, followed by a band of increased radially in the more superficial layers of the cortex and ending with a band of multicomponent in the voxels at the pial surface. Again, V2 does not show this pronounced layered structure in the FODs.

[Insert Figures 5 and 6 here]

Diffusion tensor metrics were quantified by plotting profiles over the cortical depth (Figure 5 and 6 for samples A and B) following the main fiber orientation on the basis of CSD tractography. In Supplementary Figure S1 an alternative approach using profiles perpendicular to the cortical surface is presented. In V1, several maxima and minima can be seen in the FA profiles (Figure 5,6a; middle column; red traces). From the pial surface to the stria of Gennari (dashed line on the minimum of the blue MGE trace), FA is relatively low with a minimum close to the stria of Gennari. Note that the FA minimum does not exactly coincide with the stria of Gennari, but for sample A the diffusivities L2-L3 do coincide (Figure 5b; lower grey traces), indicating hindrance of diffusion in the directions

perpendicular to the principal diffusion direction. For sample A, two more FA minima are seen in the deeper layers of the cortex. One is close to the GMWM boundary, while the other is halfway between the GMWM boundary and the stria of Gennari. The MD profile (Figure 5b) shows two minima over the cortical depth for sample A: one nearly aligned to the stria of Gennari and one near the pial surface. For sample B, the FA minimum near the stria of Gennari can also be observed, but this profile does not clearly show the other minima. The results for V2 cortex (Figure 5,6; lower panels) are highly similar between the samples, but very different from what was observed in V1. The FA profiles in V2 show a single peak over the cortical depth, skewed to the side of the pial surface. Diffusivities (Figure 5,6d) gradually drop from pial surface to GMWM boundary, but L1 is more sustained in the central layers of the cortex, as such underlying the peak in FA.

4 Discussion

The properties of the layers of the human cortex have extensively been investigated since 1776, when Gennari first observed cortical layers in *ex vivo* specimens of primary visual cortex. Nowadays, MRI methods are available to probe cortical laminar structure, even *in vivo*. Our study shows laminar patterns in the adult human neocortex *ex vivo* with Diffusion Weighted Imaging. The detail at which the layers are differentiated and characterized has not been reported before. The diffusion characteristics observed in the various layers in our V1 samples can be well accounted for by the constituents of the cortex as they have been determined in the past centuries using histological methods.

The interpretation of grey matter diffusion data we present here calls for different considerations compared to discussing white matter diffusion imaging. Ensemble diffusion anisotropy originates from non-randomly distributed elongated neural processes, i.e. axons and dendrites. Whereas the white matter consists of relatively coherent bundles of myelinated axons, the constituents of the cortex are far more heterogeneous in their size, shape and orientation. The large volume fraction occupied by somata of neurons and glia increases the isotropic diffusion compartment compared to white matter fibre bundles. Dendrites are only partially coherently organized and their contribution to the ensemble diffusion attenuation is uncertain. Axons are inhomogeneously distributed over the cortex, i.e. according to the laminar pattern, and can be myelinated or unmyelinated. Consequently, while the inference of white matter tracts is already complex, even though they contain mostly myelinated axons in perhaps 1-3 coherent fibre populations within any voxel, it is far more difficult to model the microstructural substrate of the cortex on the basis of diffusion measurements.

Nevertheless, the layer-specific diffusion properties that we observed in our cortical samples can be well accounted for by known anatomy. The layered architecture of the cortical sheet suggest that the ensembles of neural processes underlying the anisotropic fraction of the diffusion signal will be either radial or tangential to the cortical sheet. Furthermore, the cyto- and myeloarchitecture of primary visual cortex are relatively well-known. The myeloarchitecture of V1 shows radially oriented bundles of myelinated axons (radii) in the deeper layers that become thinner in layer III and disappear completely at the level of layer II. In addition, three tangential myelinated layers weave a grid with the radii (Peters and Sethares, 1996). The plexus of Exner is located in the lower part of layer I. The stria of Gennari (or outer band of Baillarger) is located in layer IVb. The inner band of Baillarger is in layer V. Layer VI also has a large amount of tangential myelinated fibres that becomes denser nearer to the underlying white matter (Vandeveldel et al., 1996). From the layers rich in pyramidal cells (VI,V,IVa,III,II), apical dendrites of pyramidal neurons co-ascend with axon radii in small bundles (Peters and Sethares, 1996).

The anisotropy in the gyral white matter of our samples is high relative to the grey matter, although not as high as reported for deep white matter *in vivo*. A decrease in anisotropy is seen at the GM-WM border, because of the crossing of tangential u-fibres with white matter fibres penetrating the cortex radially. The low anisotropy persists in the innermost band of the cortex, as both radial and tangential fibres are present in layer VI. The second dip observed in the FA profile is likely due to the inner band of Baillarger in layer V. It must be noted that we did not observe this layer clearly

throughout our samples (e.g. it is not apparent in the profile of Sample B: Figure 6b). Possibly, sometimes this layer appears continuous with layer VI at the resolution used here (0.3 mm isotropic). Gennari might have been confronted with the same problem. He observed sometimes two lines, but sometimes one line in his preparations. Baillarger (1840) speculates that the inner band of Baillarger sometimes appears continuous with layer VI and the white matter, leaving only the stria of Gennari as an intracortical band. The stria of Gennari itself is recognizable throughout the samples in the FA, MD and MGE images. In the FA image, it is seen as a conspicuous band of low FA, presumably as a result of the crossing of tangentially oriented myelinated axons and radially oriented axons/dendrites ascending to layers IVa/III/II. We have noticed a mismatch in cortical depth between the stria of the Gennari in the MGE and the expected minimum in the FA profiles. This is likely due to a composite effect of two factors that reduce FA. First, in the stria of Gennari the tangential fiber component increases. This is indicated by a reduction in L2-L3 diffusivity. For sample A, the peaks in L2-L3 line up exactly with the stria of Gennari. Second, at the same depth the L1 component decreases as radial neurites become thinner and sparser towards the pial surface. Diffusivity also increases over the superficial layers, leading to the rising edge in L1-L3. Presumably yet another composite effect of changing cell types over layers, strong reduction of the tangential neurites and gradual reduction of the radial neurites over the superficial layers going towards the pial surface. This then results in a L1 minimum that is not aligned with the stria of Gennari. The superposition of these effects is likely to have a minimum that also does not exactly coincide with the center of the stria of Gennari. In sample B, the same pattern is seen in the peaks of the L1-L3 diffusivity, i.e. a shift of the L1 minimum towards the pial surface compared to L2-L3. However, the peaks in L2-L3 do not line up with the stria of Gennari, but the L1-L3 peaks are shifted towards the GMWM boundary. This leads us to suspect that an additional and alternative explanation for the mismatch of the peaks is plausible here: that the registration and unwarping procedure might not have been sufficiently accurate for this area of sample B. It appears that a shift of the profiles of all diffusion metrics towards the pial surface increases the similarity between the profiles of sample A and B. Finally, within the superficial layers, a minor dip in L2-L3 is observed near the pial surface that is more pronounced for L2-L3, which could correspond to the stripe of Kaes-Bechterew formed by tangential dendritic collaterals.

Other studies before ours have looked at diffusion characteristics of the grey matter of the cortex. While the early studies in animals focused on ADC reductions in ischemic tissue, cortical anisotropy was already noted (Hoehn-Berlage et al., 1995, 1999; Lythgoe et al., 1997; Thornton et al., 1997). At the turn of the previous century, cortical DWI investigations were mostly aimed at characterizing cortical development (McKinstry et al., 2002; Mori et al., 2001; Neil et al., 1998). The approach is well suited for this purpose as cortical anisotropy varies over gestational age and reflects microstructural events in neurodevelopment (McKinstry et al., 2002). Therefore, it has persisted as a tool for investigating cortical development (Huang et al., 2008; Kroenke et al., 2005, 2007, 2009; Maas et al., 2004; Sizonenko et al., 2007; Takahashi et al., 2011). These studies are very relevant in the context of our findings, as they provide convincing empirical evidence of the suggested microstructural substrates of our adult cortical diffusion data. The radial anisotropy observed in the developing cortex is thought to stem mainly from radial glia that serve as scaffolding for the cortical neurons that migrate from the ventricular zone. Over the period of cortical maturation, these radial glia are replaced by radial and basal dendrites with elaborate arborisations forming local cortical circuits. This results in a marked reduction in anisotropic structure (McKinstry et al., 2002).

Interestingly, the FA reduction follows a similar temporal pattern as the morphological maturation of pyramidal neurons, suggesting that pyramidal dendrites and axons are the main determinant of the cortical diffusion signal (Kroenke et al., 2009).

To the authors' knowledge, differential diffusion properties of cortical layers were first reported in the mouse brain by Wedeen et al. (2004). Not only did they show variations in the planar architecture of cortical layers, they also noted differences over areas of the cortex. FA differences have been shown between the deep and superficial layers of the developing mouse (Sizonenko et al., 2007) and ferret (Kroenke et al., 2009) brain. The layer-specific nature of cortical diffusion has got little attention outside the literature on cortical development, probably because *in vivo* cortical diffusion studies have been outside the realm of possibilities. Recently, Dyrby et al. (2011) have shown a subdivision in diffusion behaviour of deep and superficial layers of the adult pig brain, where the deeper layers showed multiple peaks of the FODs and the outer layers a purely radial orientation. The fact that a more elaborate laminar pattern was seen in our human tissue samples could be due to our better resolution and/or differences between human and bovine cortex. In addition, their study showed an elegant demonstration of the layers of the hippocampus. The human hippocampus was investigated *ex vivo* showing a very detailed subdivision of the hippocampal layers in diffusion tensor metric maps (Shepherd et al., 2007). In recent years, studies have convincingly reported cortical anisotropy with radially oriented diffusion tensors in humans, both *ex vivo* (Benner et al., 2009; McNab et al., 2009) and *in vivo* (Heidemann et al., 2010; Jaermann et al., 2008). This suggests that the dominant diffusion orientation pooled over the cortical depth is radial. This is confirmed by our data. Other work has already suggested that this radially does not show equally in all cortical regions (McNab et al., 2011). That the cortical diffusion profile varies over cortical areas is also something that our data indicate. Profiles obtained from V1 were distinctly different from those of V2. If diffusion profiles represent a superposition of the radial and tangential components of the various cortical layers, it is bound to vary over Brodmann areas and will also be reflected in the diffusion tensor. Finally, in a design much like our own, Leuze et al. (2011) have shown layer-specific diffusion properties in the stria of Gennari. They reported radial orientation of the diffusion tensor in the cortex, but a breakdown of this radially in the stria of Gennari. Interestingly, they noted that the orientation in the outermost cortical voxels was tangential to the cortex. We have not been able to observe this reliably in our data. Possibly, this results from the better in-plane resolution of their data, while we have used data with isotropic voxel size.

Regarding the methods used, some technical limitations have to be considered. Susceptibility artefacts can cause distortion, especially at high field. This results in geometric differences between the anatomical reference MGE image and the DWI images. A segmented EPI read-out was used and EPI images were corrected by warping them to the MGE image to minimize distortions. Nonetheless, as already mentioned some mismatch between DWI and MGE layers cannot be excluded. Our samples were immersed in a proton-free liquid during scanning, causing a sharp drop in intensity at the outer boundary of the sample, which can give rise to Gibbs ringing. In MRI, Gibbs ringing manifests itself as an oscillating intensity variation in one direction, potentially resembling cortical layers (Koopmans et al., 2008). However, this is a rather unlikely explanation of the laminar pattern in our samples. Cortical areas not at an interface (but directly bordered by a neighbouring gyrus) also show the same layered appearance in the cortex. Furthermore, the largest dip in the profile (the stria of Gennari) is seen multiple voxels from the sample boundary, while the largest Gibbs effect would be expected in the voxels directly adjacent to the boundary. Finally, while *in vivo* DWI already

suffers from low SNR, the short T_2 and low diffusivity in *ex vivo* DWI makes this even worse. To achieve the resolution presented in this paper, ultra-high field strength and use of highly sensitive coils are prerequisites. Moreover, we were able to overcome the unfavourable SNR conditions by acquiring the DWI with many repetitions and gradient directions.

We have acquired the diffusion data on a single shell with a b-value of 4000 sec/mm². For the diffusion tensor and derived metrics presented in this paper, this will have sufficed. However, for the reconstruction of the FODs a multishell acquisition is probably more optimal. We have included fiber orientation distribution images primarily to show the main diffusion direction in our samples. These main peaks of the FODs resemble the principal diffusion direction from the diffusion tensor very well and highlight the radial diffusion orientation in the cortex. At the same time, these FODs show multiple components in areas where the diffusion tensor formalism does not hold. In our samples, these are, most notably, the areas of u-fibres and the cortex with the stria of Gennari in particular. Although some of the secondary components seem to follow the expected anatomy, in general we do not believe that the FODs in the cortex represent the true underlying fiber configurations accurately. For example, in the stria of Gennari and other cortical layers, many two-component FODs are observed with one component in the radial direction and one component in a tangential direction. This is not a plausible fiber configuration for cortical tissue, where instead a radial component is expected, but the tangential component is more likely to be equally distributed over all directions in the tangential plane. This secondary component could then be either true, in the sense that the tangential fibres might actually not be homogeneously distributed, or the component could be spurious. The deconvolution technique relies on estimation of a response function to single coherent fiber configurations. Although this appears to be the case judging from the many single component FODs in our images, the low FA in our (<0.4) suggests otherwise. By using a response function estimated from low-FA voxels, we reduce the sensitivity to find multicomponent FODs. Furthermore, deconvolution can generate spurious components when estimating the response function on the basis of voxels with low FA (Parker and Jones, 2011). To investigate whether the multicomponent FODs might be an artefact of the method used, we have performed q-ball and persistent angular structure (PAS) reconstructions of the same data. The results are provided in Supplementary Figure S2. We conclude that whilst most voxels show similarity in the reconstructed directions, many areas of multicomponent reconstructions do not arrive at the same result and the amount of multicomponent voxels depends heavily on the method chosen and the filter settings used. This has been well known in the diffusion modelling community, but is extra relevant in our *ex vivo* data. Improved modelling approaches that are better suited to the cortex are necessary to resolve the fiber configurations in our data. Some steps in this direction have already been taken. For example, Zhang et al. (2012) specifically model neurite orientation dispersion and density in white matter as well as grey matter. Another useful improvement in this respect was proposed by Dell'Acqua et al. (2010) who account for the isotropic partial volume component in spherical deconvolution approaches.

We foresee some clinical applications in characterizing abnormalities that occur in diseases affecting the cortex. Recent papers have shown cortical FA and ADC changes in MS (Vrenken et al., 2006), ALS (Senda et al., 2011) and Alzheimer's disease (Canu et al., 2011). Layer-specific information on microstructure, either *in vivo* or *ex vivo*, could identify what underlies these changes. One of the more interesting potential research applications of cortical diffusion imaging is cortical architectonic mapping. Other MRI contrasts that are sensitive to myelination have already been used as *in vivo*

histological markers (Barazany and Assaf, 2011; Cohen-Adad et al., 2012; Glasser and Van Essen, 2011). Admittedly, it is much more problematic to achieve the required resolution in DWI due to its intrinsically low SNR. However, disregarding the technical difficulties for now and in expectance of further technical improvements, DWI is pre-eminently suited for *in vivo* investigation of cortical microstructure, and thus cyto- and myeloarchitecture. Potentially, it can quantify radial and tangential fibre components, as well as cell and axon size distributions in cortical layers or areas. Furthermore, our results might be informative for future tractography applications. The radial cortical anisotropy observed at high resolutions has already been used for tracking fibres from the white matter into the cortex (Heidemann et al., 2011; Takahashi et al., 2010; Wedeen et al., 2005, 2008), which was not possible before. Layer-specific results might provide clues to determine the input-output layers of cortical area, thus define the correct layers for termination of tractography. It would mean a substantial improvement in the assessment of brainwide networks with DWI. One could even speculate on reconstructing intracortical circuits with tractography.

We conclude that for diffusion imaging in the cortex, the contributions of the various layers of the cortex should be considered. We realise that the resolution reported on in the present paper is not sufficient to resolve cortical layers that are no more than a few tens of microns thick. Nevertheless, we hope that the results presented in this paper are a mere starting point for further investigations into the diffusion characteristics of cortical layers. Provided efforts to progress in high-resolution diffusion imaging continue, one day we might even see *in vivo* DWI of cortical layers. As for many emerging techniques investigating the cortex, the stria of Gennari is probably the first thing we would be able to see. More than two centuries after its discovery the stria of Gennari still has its appeal in neuroscience.

5 References

Baillarger JGF. Recherches sur la structure de la couche corticale des circonvolutions du cerveau.

Mémoires de l'Académie royale de Médecine de Paris, 8:149-183, 1840.

Barazany D and Assaf Y. Visualization of cortical lamination patterns with magnetic resonance imaging. *Cerebral Cortex*, 2011.

Barbier EL, Marrett S, Danek A, Vortmeyer A, van Gelderen P, Duyn J, Bandettini P, Grafman J, and Koretsky AP. Imaging cortical anatomy by high-resolution MR at 3.0T: detection of the stripe of Gennari in visual area 17. *Magnetic Resonance in Medicine*, 48 (4):735-738, 2002.

Benner T, Bakkour A, Wang R, and Dickerson BC. High resolution ex-vivo diffusion imaging and fiber tracking. *Proceedings of the International Society for Magnetic Resonance in Medicine*, 17:3535, 2009.

Blackwell ML, Farrar CT, Fischl B, and Rosen BR. Target-specific contrast agents for magnetic resonance microscopy. *NeuroImage*, 46 (2):382-393, 2009.

Blum F. Der formaldehyd als hartungsmittel. *Z. Wiss. Mikrosk.*, 10, 314-315, 1893.

Bridge H, Clare S, Jenkinson M, Jezzard P, Parker AJ, and Matthews PM. Independent anatomical and functional measures of the V1/V2 boundary in human visual cortex. *Journal of Vision*, 5 (2):93-102, 2005.

Brodmann K. Beiträge zur histologischen Lokalisation der Grosshirnrinde: dritte Mitteilung: Die Rindenfelder der niederen Affen. *Journal für Psychologie und Neurologie*, 4:177-226, 1905.

Brodmann K. *Vergleichende Lokalisationslehre der Grosshirnrinde in ihren Prinzipien dargestellt auf Grund des Zellenbaues*. Leipzig: Johann Ambrosius Barth Verlag, 1909.

Canu E, McLaren DG, Fitzgerald ME, Bendlin BB, Zoccatelli G, Alessandrini F, Pizzini FB, Ricciardie GK, Beltramelloe A, Johnson SC, and Frisoni GB. Mapping the structural brain changes in Alzheimer's disease: the independent contribution of two imaging modalities. *Journal of Alzheimer's disease*, 26 (Suppl 3):263-274, 2011.

Cohen-Adad J, Polimeni JR, Helmer KG, Benner T, McNab JA, Wald LL, Rosen BR, and Mainero C. T_2^* mapping and B_0 orientation-dependence at 7T reveal cyto- and myeloarchitecture organization of the human cortex. *NeuroImage*, in press.

Cook PA, Bai Y, Seunarine KK, Hall MG, Parker GJ, and Alexander DC. Camino: open-source diffusion-MRI reconstruction and processing. *Proceedings of the International Society for Magnetic Resonance in Medicine*, 14:2759, 2006.

Cook PA, Symms M, Boulby PA, Alexander DC. Optimal acquisition orders of diffusion-weighted MRI measurements. *Journal of Magnetic Resonance Imaging*, 25 (5): 1051-1058, 2007.

D'Arceuil H, de Crespigny A. The effects of brain tissue decomposition on diffusion tensor imaging and tractography. *Neuroimage* 36 (1): 64-68, 2007.

Dell'Acqua F, Scifo P, Rizzo G, Catani M, Simmons A, Scotti G, Fazio F. A modified damped Richardson-Lucy algorithm to reduce isotropic background effects in spherical deconvolution. *Neuroimage* 49 (2), 2010.

Dyrby TB, Baaré WFC, Alexander DC, Jelsing J, Garde E, and Sjøgaard LV. An ex vivo imaging pipeline for producing high-quality and high-resolution diffusion-weighted imaging datasets. *Human brain mapping*, 32 (4):544-563, 2011.

Gennari F. *De peculiari structura cerebri, nonnullisque ejus morbi*. Parma: Ex Regio Typographeo, 1782.

Glasser MF and Van Essen DC. Mapping human cortical areas in vivo based on myelin content as revealed by T1- and T2-weighted MRI. *Journal of Neuroscience*, 31 (32):11597-11616, 2011.

Glickstein M and Rizzolatti G. Francesco Gennari and the structure of the cerebral cortex. *Trends in Neurosciences*, 7 (12):464-467, 1984.

Golgi C. Sulla struttura della sostanza grigia del cervello. *Gazzetta Medica Italiana*, 33:244-246, 1873.

Heidemann RM, Anwander A, Feiweier T, Grinstead J, Lohmann G, Knösche TR, and Turner R. k-space and q-space: combining ultra-high spatial and angular resolution in diffusion imaging using ZOOPPA at 7T. *Proceedings of the International Society for Magnetic Resonance in Medicine*, 19:1957, 2011.

Heidemann RM, Porter DA, Anwander A, Feiweier T, Heberlein K, Knösche TR, and Turner R. Diffusion imaging in humans at 7T using readout-segmented EPI and GRAPPA. *Magnetic Resonance in Medicine*, 64 (1):9-14, 2010.

Hoehn-Berlage M, Eis M, Back T, Kohno K, and Yamashita K. Changes of relaxation times (T1, T2) and apparent diffusion coefficient after permanent middle cerebral artery occlusion in the rat: temporal evolution, regional extent, and comparison with histology. *Magnetic Resonance in Medicine*, 34 (6):824-834, 1995.

Hoehn-Berlage M, Eis M, and Schmitz B. Regional and directional anisotropy of apparent diffusion coefficient in rat brain. *NMR in Biomedicine*, 12:45-50, 1999.

Huang H, Yamamoto A, Hossain MA, Younes L, and Mori S. Quantitative cortical mapping of fractional anisotropy in developing rat brains. *The Journal of Neuroscience*, 28 (6):1427-1433, 2008.

Jaermann T, De Zanche N, Staempfli P, Pruessmann KP, Valavanis A, Boesiger P, and Kollias SS. Preliminary experience with visualization of intracortical fibres by focused high-resolution diffusion tensor imaging. *American Journal of Neuroradiology*, 29 (1):146-50, 2008.

- Jones DK, Horsfield MA, Simmons A. Optimal strategies for measuring diffusion in anisotropic systems by magnetic resonance imaging. *Magnetic Resonance in Medicine* 42 (3), 1999.
- Koopmans PJ, Manniesing R, Niessen WJ, Viergever MA, and Barth M. MR venography of the human brain using susceptibility weighted imaging at very high field strength. *Magnetic Resonance Materials in Physics, Biology and Medicine*, 21 (1-2):149-158, 2008.
- Koopmans PJ, Barth M, and Norris DG. Layer-specific BOLD activation in human V1. *Human Brain Mapping*, 31 (9):1297-1304, 2010.
- Kroenke CD, Bretthorst GL, Inder TE, and Neil JJ. Diffusion MR imaging characteristics of the developing primate brain. *Neuroimage*, 25 (4):1205-1213, 2005.
- Kroenke CD, Taber EN, Leigland LA, Knutsen AK, and Bayly PV. Regional patterns of cerebral cortical differentiation determined by diffusion tensor MRI. *Cerebral Cortex*, 19 (12):2916-2929, 2009.
- Kroenke CD, Van Essen DC, Inder TE, Rees S, Bretthorst GL, and Neil JJ. Microstructural changes of the baboon cerebral cortex during gestational development reflected in magnetic resonance imaging diffusion anisotropy. *The Journal of Neuroscience*, 27 (46):12506-12515, 2007.
- Leuze C, Dhital B, Anwender A, Pampel A, Heidemann RM, Geyer S, Gratz M, and Turner R. Visualization of the orientational structure of the stria of Gennari with high-resolution DWI. *Proceedings of the International Society for Magnetic Resonance in Medicine*, 19:2371, 2011.
- Lythgoe MF, Busza AL, Calamante F, Sotak CH, King MD, Bingham AC, Williams SR, and Gadian DG. Effects of diffusion anisotropy on lesion delineation in a rat model of cerebral ischemia. *Magnetic Resonance in Medicine*, 38 (4):662-668, 1997.
- Maas LC, Mukherjee P, Carballido-Gamio J, Veeraraghavan S, Miller SP, Partridge SC, Henry RG, Barkovich AJ, and Vigneron DB. Early laminar organization of the human cerebrum demonstrated with diffusion tensor imaging in extremely premature infants. *NeuroImage*, 22:1134-1140, 2004.

McKinstry RC, Mathur A, Miller JH, Ozcan A, Snyder AZ, Schefft GL, Almli CR, Shiran SI, Conturo TE, Neil JJ. Radial organization of developing preterm human cerebral cortex revealed by non-invasive water diffusion anisotropy MRI. *Cerebral Cortex*, 12 (12):1237-1243, 2002.

McNab JA, Jbabdi S, Deoni SCL, Douaud G, Behrens TEJ, and Miller KL. High resolution diffusion-weighted imaging in fixed human brain using diffusion-weighted steady state free precession. *NeuroImage*, 46 (3):775-85, 2009.

McNab JA, Polimeni JR, Wald LL. Surface based analysis of diffusion orientation for identifying architectonic domains in the in vivo human cortex. *Proceedings of the International Society for Magnetic Resonance in Medicine*, 19:412, 2011.

Mori S, Itoh R, Zhang JY, Kaufmann WE, van Zijl PCM, Solaiyappan M, and Yarowsky P. Diffusion tensor imaging of the developing mouse brain. *Magnetic Resonance in Medicine*, 46 (1):18-23, 2001.

Neil JJ, Shiran SI, McKinstry RC, Schefft GL, Snyder AZ, Almli CR, Akbudak E, Aronovitz JA, Miller JP, Lee BC, and Conturo TE. Normal brain in human newborns: apparent diffusion coefficient and diffusion anisotropy measured by using diffusion tensor MR imaging. *Radiology*, 209 (1):57-66, 1998.

Parker G, Jones D. Fibres at the Magic Angle Generated by Inappropriate Calibration (MAGIC). *Proceedings of the International Society for Magnetic Resonance in Medicine*, 18:1921, 2011.

Peters A and Sethares C. Myelinated axons and the pyramidal cell modules in monkey primary visual cortex. *The Journal of Comparative Neurology*, 365:232-255, 1996.

Senda J, Kato S, Kaga T, Ito M, Atsuta N, Nakamura T, Watanabe H, Tanaka F, Naganawa S, and Sobue G. Progressive and widespread brain damage in ALS: MRI voxel-based morphometry and diffusion tensor imaging study. *Amyotrophic Lateral Sclerosis*, 12 (1):59-69, 2011.

Shepherd TM, Ozarslan E, Yachnis AT, King MA, Blackband SJ. Diffusion tensor microscopy indicates the cytoarchitectural basis for diffusion anisotropy in the human hippocampus. *American Journal of Neuroradiology*, 28 (5): 958-964, 2007.

Shepherd TM, Thelwall PE, Stanisiz GJ, Blackband SJ. Aldehyde Fixative Solutions Alter the Water Relaxation and Diffusion Properties of Nervous Tissue. *Magnetic Resonance in Medicine*, 62 (1): 26-34, 2009.

Sizonenko SV, Camm EJ, Garbow JR, Maier SE, Inder TE, Williams CE, Neil JJ, and Huppi PS. Developmental changes and injury induced disruption of the radial organization of the cortex in the immature rat brain revealed by in vivo diffusion tensor MRI. *Cerebral Cortex*, 17 (11):2609-2617, 2007.

Takahashi E, Dai G, Rosen GD, Wang R, Ohki K, Folkerth RD, Galaburda AM, Wedeen VJ, and Grant PE. Developing neocortex organization and connectivity in cats revealed by direct correlation of diffusion tractography and histology. *Cerebral Cortex*, 21 (1):200-211, 2011.

Takahashi E, Dai G, Wang R, Ohki K, Rosen GD, Galaburda AM, Grant PE, and Wedeen VJ. Development of cerebral fiber pathways in cats revealed by diffusion spectrum imaging. *NeuroImage*, 49 (2):1231-1240, 2010.

Thornton JS, Ordidge RJ, Penrice J, Cady EB, Amess PN, Punwani S, Clemence M, and Wyatt JS. Anisotropic water diffusion in white and gray matter of the neonatal piglet brain before and after transient hypoxia-ischaemia. *Magnetic Resonance Imaging*, 15 (4), 433-440, 1997.

Tournier J-D, Calamante F, and Connelly A. Robust determination of the fibre orientation distribution in diffusion MRI: non-negativity constrained super-resolved spherical deconvolution. *NeuroImage*, 35 (4):1459-1472, 2007.

- Trampel R, Ott DVM, and Turner R. Do the congenitally blind have a stria of Gennari? First intracortical insights in vivo. *Cerebral Cortex*, 21 (9):2075-2081, 2011.
- Turner R, Oros-Peusquens A-M, Romanzetti S, Zilles K, and Shah NJ. Optimised in vivo visualisation of cortical structures in the human brain at 3 T using IR-TSE. *Magnetic Resonance Imaging*, 26 (7):935-42, 2008.
- Vandeveldel IL, Duckworth E, and Reep RL. Layer VII and the gray matter trajectories of corticocortical axons in rats. *Anatomy and Embryology*, 194 (6):581-593, 1996.
- Visser E, Qin S, and Zwiers MP. EPI distortion correction by constrained nonlinear coregistration improves group fMRI. *Proceedings of the International Society for Magnetic Resonance in Medicine*, 18:3459, 2010.
- Vrenken H, Pouwels PJW, Geurts JJG, Knol DL, Polman CH, Barkhof F, and Castelijns JA. Altered diffusion tensor in multiple sclerosis normal-appearing brain tissue: cortical diffusion changes seem related to clinical deterioration. *Journal of Magnetic Resonance Imaging*, 23 (5):628-636, 2006.
- Wedeen VJ, Song S, Wald L, Reese TG, Benner T, and Tseng W. Diffusion spectrum MRI of cortical architectonics: visualization of cortical layers and segmentation of cortical areas by analysis of planar structure. *Proceedings of the International Society for Magnetic Resonance in Medicine*, 11:622, 2004.
- Wedeen VJ, Wang RP, Schmahmann JD, Benner T, Tseng WY, Dai G, Pandya DN, Hagmann P, D'Arceuil H, and de Crespigny AJ. Diffusion spectrum magnetic resonance imaging (DSI) tractography of crossing fibres. *NeuroImage*, 41 (4): 1267-1277, 2008.
- Weigert C. Ausführliche Beschreibung der in No. 2 dieser Zeitschrifterwasnten neuen Farbungsmethod fur das Centralnervensystem. *Fortschr. Deutsch. Med.*, 2:190-191, 1884.

Zhang H, Schneider T, Wheeler-Kingshott CA, Alexander DC. NODDI: Practical in vivo neurite orientation dispersion and density imaging of the human brain. *Neuroimage* 61 (4), 2012.

Zwiers MP. Patching cardiac and head motion artefacts in diffusion-weighted images. *NeuroImage*, 53 (2):565-575, 2010.

ACCEPTED MANUSCRIPT

Figure 1. Title page and plate from Francesco Gennari's 'De Peculiaribus Structura Cerebri'. a) In 1782 Francesco Gennari published his treatise on the anatomy of the brain. b) In his work, Gennari described the 'lineola albidior' (white line), most distinct in the part of the brain over the tentorium, i.e. the occipital lobe. The red dotted lines on the pial surface outline the regions where the stria of Gennari is visible.

Figure 2. Nineteenth century investigations into the layered structure of the neocortex. a) Jules Gabriel François Baillarger (1809-1890). b) Baillarger identified six layers in the cortex of alternating grey-white appearance as shown in the inset. The inner white layers (2,4; incrementing from WM to pial) are referred to as the inner and outer band of Baillarger. In primary visual cortex the outer band of Baillarger is synonymous with the stria of Gennari. c) Theodor Hermann Meynert (1833-1892), founder of the field of cortical architectonics. d) Meynert's classification of the cortex in the calcarine sulcus into eight layers.

Figure 3. Maps of diffusion metrics for Sample A. Two orthogonal slice orientations are shown in the upper and lower panel. a,g) MGE maps: dash-dotted lines indicate the WM boundary; lines in the cortex indicate V1/V2 boundaries; dashed lines spanning the figure indicate the position of the slice in the lower panel. b,h) MD maps: boxes indicate the areas of (e,f/k,l); arrows indicate where u-fibers are most prominent. c,i) FA maps; arrows highlight some cortical layers of low FA. d,j) DEC maps, interpolated to accentuate the layered structure of the cortex. e) FODs in a section of V1 cortex: dashed lines propose a putative division into separable layers. f) FODs in a section of V2 cortex. k,l) FODs in a section of V1 cortex at different magnifications. FODs are overlain on FA maps.

Figure 4. Maps of diffusion metrics for Sample B. Refer to the caption of Figure 3 for the description of the figure layout.

Figure 5. Cortical profiles of diffusion metrics for Sample A. The upper panel shows profiles from V1; the lower panel shows the profiles from V2. Panels are divided in an upper and lower row showing FA (a,c) and diffusivity (b,d) profiles, respectively (red traces). MGE profiles (blue traces) are included in every graph for reference of cortical architecture. Dotted lines indicate the standard deviation over the MGE, FA and MD profiles. In the diffusivity graphs (b,d) the grey dash-dotted traces represent the diffusion tensor eigenvalues L1-L3. The leftmost graphs are scaled identically for each panel to facilitate comparison between Sample A/B and V1/V2. The location of the GMWM boundary is indicated by the vertical dash-dotted line. The graphs in the middle column have the same scaling on the Y-axis, but various offsets, in order to visualize the relevant parts of the curves. The X-axis has been scaled such that the full axis equals the cortical depth from pial surface (left) to GMWM boundary (right). The right column shows sampling regions and the images sampled. h) fiber tracts from the pial surface of a patch V1 cortex (red seed region; green streamlines) and a patch of V2 cortex (yellow seed region; red streamlines) overlaid on the MGE image. For each region, the FA map (f,i) and MD map (g,j) are shown next to their graph, complemented with the DEC map overlaid with FODs (e,k) in the right upper and lower corner. SOG=Stria of Gennari.

Figure 6. Cortical profiles of diffusion metrics for Sample B. Refer to the caption of Figure 5 for the description of the figure layout.

Supplementary Figure 1. Cortical profiles of diffusion metrics. Separate pages show results for Sample A and B. On each page, the upper panel shows profiles from V1; the lower panel shows the

profiles from V2. Panels are divided in an upper and lower row showing FA (a,c) and diffusivity (b,d) profiles, respectively (red traces). MGE profiles (blue traces) are included in every graph for reference of cortical architecture. Dotted lines indicate the standard deviation over the MGE, FA and MD profiles. In the diffusivity graphs (b,d) the grey dash-dotted traces represent the diffusion tensor eigenvalues L1-L3. The leftmost graphs are scaled identically for each panel to facilitate comparison between samples and V1/V2. The location of the GMWM boundary is indicated by the vertical dash-dotted line. The graphs in the middle column have the same scaling on the Y-axis, but various offsets, in order to visualize the relevant parts of the curves. The X-axis has been scaled such that the full axis equals the cortical depth from pial surface (left) to GMWM boundary (right). The right column shows sampling regions and the images sampled. h) fiber tracts from the pial surface of a patch V1 cortex (red seed region; green streamlines) and a patch of V2 cortex (yellow seed region; red streamlines) overlaid on the MGE image. For each region, the FA map (f,i) and MD map (g,j) are shown next to their graph complemented with the DEC map overlaid with FODs (e,k) in the right upper and lower corner. SOG=Stria of Gennari.

In this supplementary figure, additional traces have been included to show the difference between the method of extracting the cortical profiles along the streamlines and extracting the cortical profiles perpendicular to the cortical surface. From the seed regions, surface normals were determined in the MGE image and sampled along a depth of 3 mm with a sampling distance of 0.03 mm. For the 'cortex normals' method the MGE is represented by the black traces, the FA and MD are represented by the yellow traces and L1-L3 by the dark grey dash-dotted traces.

Not surprisingly, the resulting profiles were very similar to the profiles obtained by sampling along the streamlines, because the FODs are mostly perpendicular to the cortex. We find that the peaks of the curve within the cortex only differ somewhat in amplitude with the peaks being a bit more pronounced for the 'cortex normals' method. In the sampled region of sample B-V1 we see a small shift in the cortical depth at which the peaks occur, because the orientation is not exactly

perpendicular to the cortical surface. Large differences start to occur when leaving the cortex as the fibers bend into the WM and sample completely different voxels. The standard deviation over the profiles is lower in the case of the 'cortex normals' method, presumably because of slight bending of the fiber tracks within the cortex.

Supplementary Figure 2. Constrained Spherical Deconvolution FODs, Q-ball and Persistent Angular Structure functions for Sample A-V1 (a-c), Sample A-V2 (d-f), Sample B-V1 (g-i) and Sample B-V2 (j-l). CSD reconstruction with spherical harmonic order 8, estimating the fiber response function from the (~7000) voxels with $FA > 0.1$ within a mask with high SNR and excluding pial boundary voxels. Q-ball (spherical harmonic order 8) and PAS reconstruction (PAS function 1.1) were performed using the Camino toolkit.

a) FRANCISCI GENNARI

PARMENSIS

MEDICINAE DOCTORIS COLLEGIATI

DE PECULIARI
STRUCTURA CEREBRI

NONNULLISQUE EJUS MORBIS .

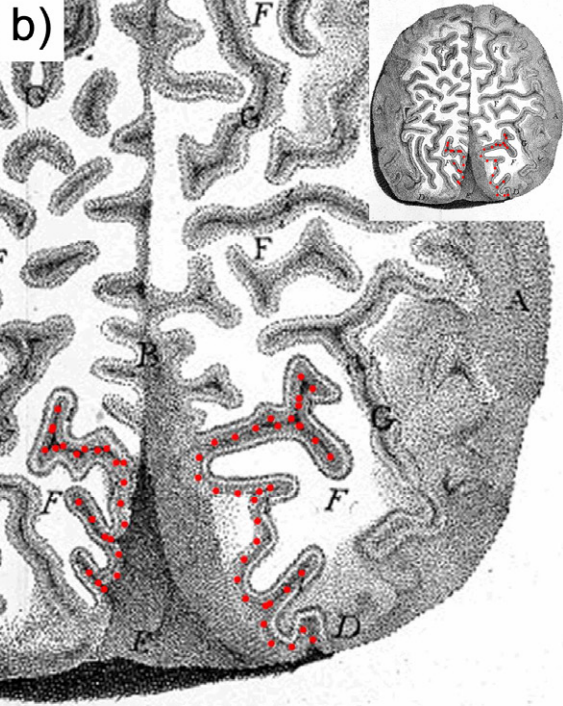
PAUCAE ALIAE ANATOM. OBSERVAT.
ACCEDUNT .

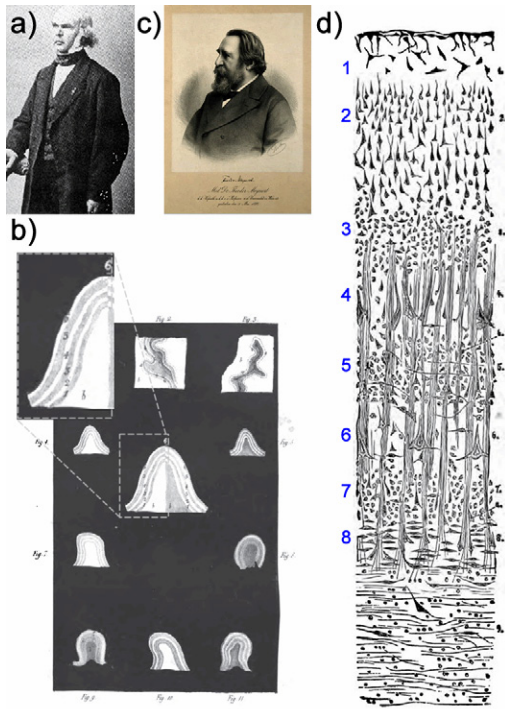
PARMAE

EX REGIO TYPOGRAPHEO

M. DCC. LXXXII.

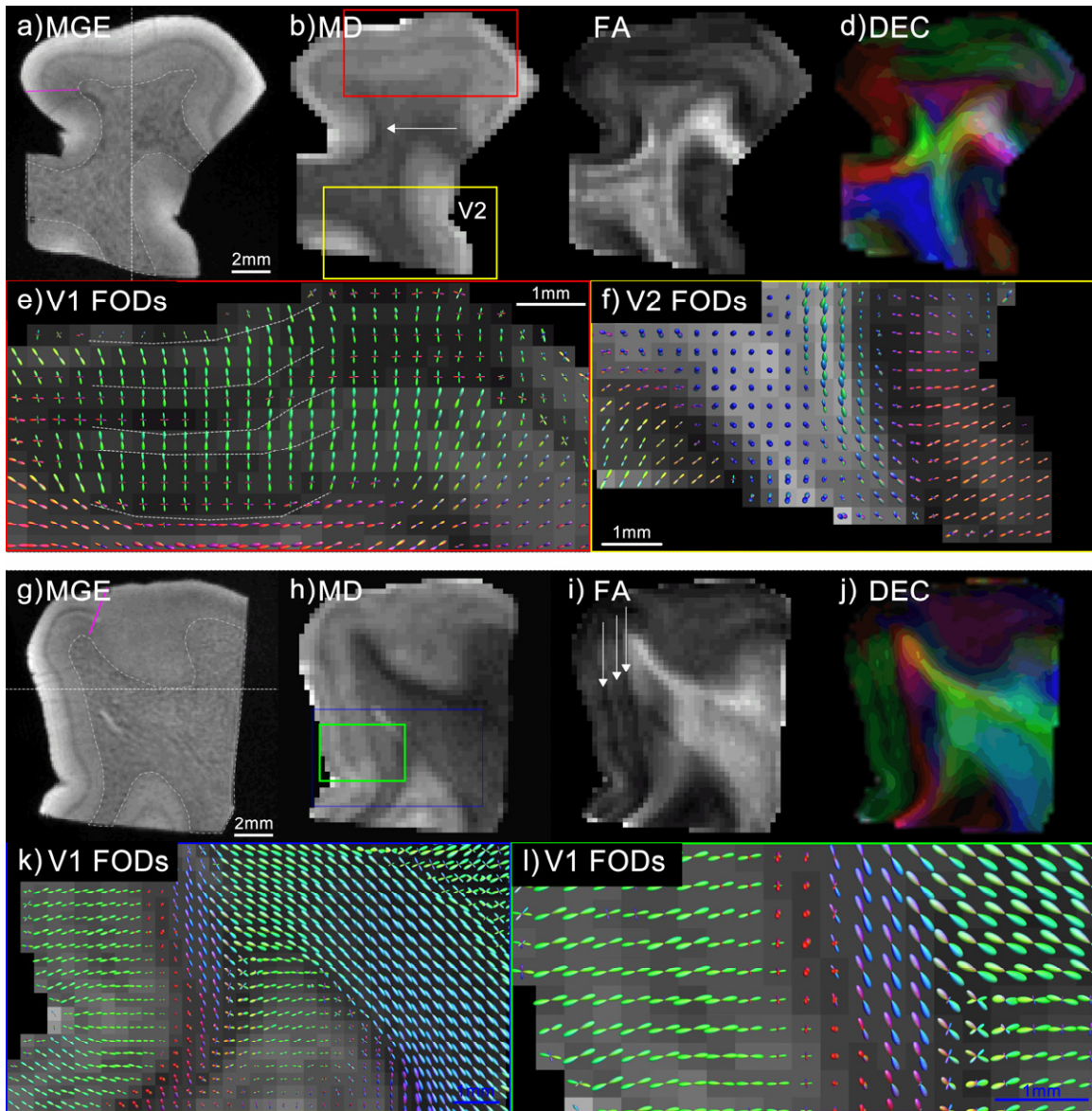
CUM APPROBATIONE .

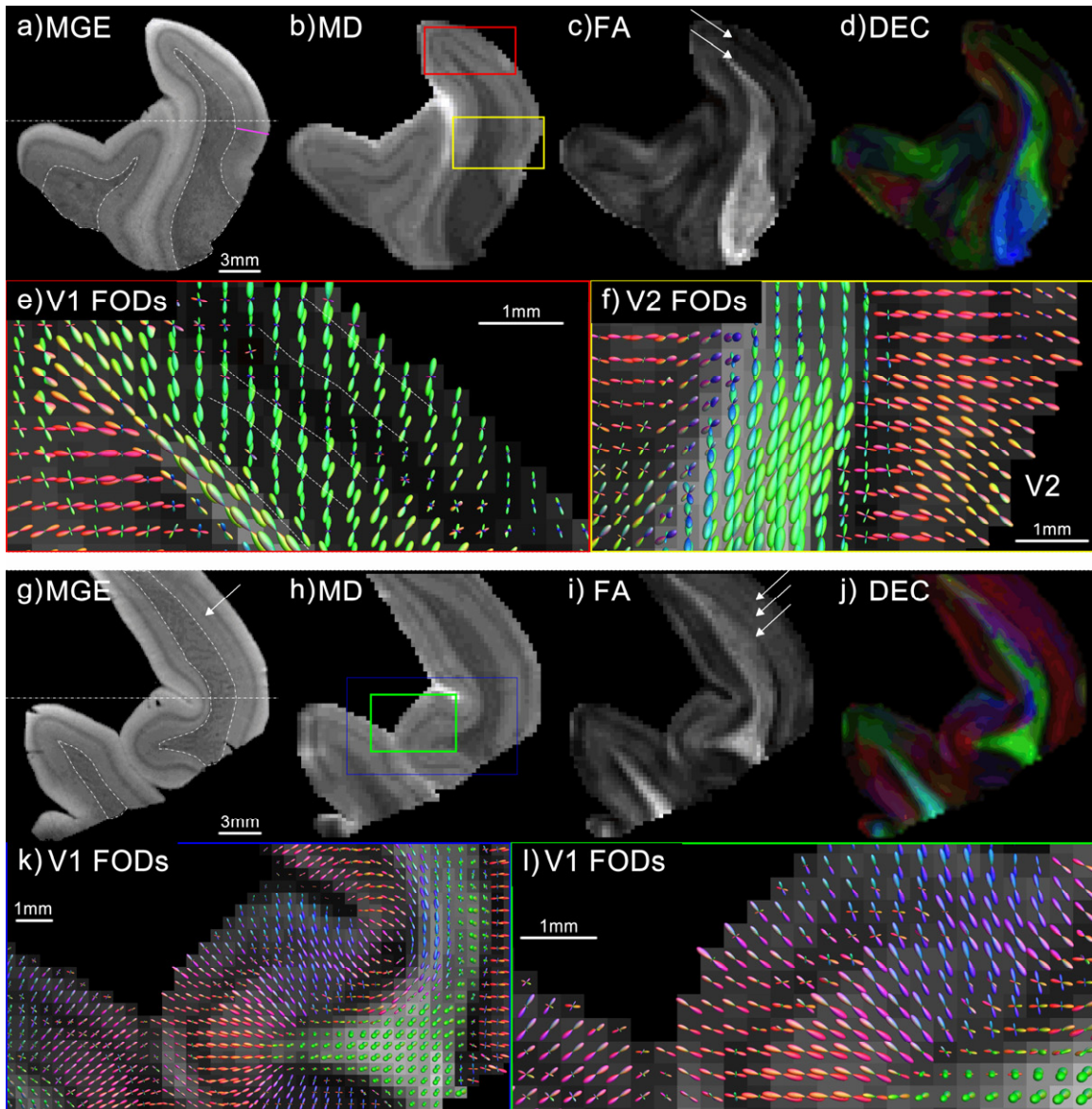




Transparent Section through the Cortex of the Calcarine Fissure.
 1. Neurons layer. 2. Layer of pyramids. 3. External granular layer. 4. External barren intergranular layer with solitary cell. 5. External granular layer. 6. External granular layer with solitary cells. 7. Inner granular layer. 8. Layer of fusiform cells. 9. Medullary substance of the convoluted.

ACCEPTED MANUSCRIPT





ACCEPTED

